Electronic Supplementary Material (ESI) for Physical Chemistry Chemical Physics.

Superior thermoelectric performances of two-dimensional Tri-Tri group-VA nanomaterials

Jia-He Lin[†], Tie Zhang[‡], and Tian Zhang [‡*]

†*School of Science, Jimei University, Xiamen 361021*

‡*School of Physics and Electronic Engineering, Sichuan Normal University, Chengdu 610066, China*

[*]*e-mail:zhangt512@foxmail.com*

ABSTRACT: High-performance thermoelectric materials in theoretical and experimental research are mostly composed of expensive, scarce heavy elements and rarely of single light elements, which severely limits their application and development. Based on density functional and semiclassical Boltzmann transport theory, we determine that a stable phosphorene allotrope, named Tri-Tri phosphorene, has super-high electron mobility (23845.29 cm^2/Vs) much higher than those of most two-dimension materials. Moreover, its optimized maximum ZT can reach up to 3.43 at room temperature (4.83 at 500 K and 5.92 at 700 K), exhibiting a highly favorable prospect in practical thermoelectric systems. Motivated by the excellent properties of Tri-Tri phosphorene, we further demonstrate the structural stability of Tri-Tri arsenene and Tri-Tri antimonene and predict that the two Tri-Tri structures also have high Seebeck coefficients and electron mobilities. Their lattice thermal conductivities are dramatically decreased compared with Tri-Tri phosphorene. Thus, their predicted thermoelectric performances are also excellent, with maximum ZT values of 4.12 (Tri-Tri arsenene) and

3.54 (Tri-Tri antimonene) at room temperature. The low layer modulus of the three Tri-Tri structures indicate that they are high mechanical flexibility and suitability for current device assemblies. All these desirable properties make Tri-Tri group-VA materials promising for future applications in thermoelectric devices.

Table S1: Calculated mechanical parameters of the monolayer Tri-Tri arsenene and Tri-Tri antimonene.

System	γ (N/m)	$\gamma_0^{'}$	$\gamma_0^{''}$ (m/N)	γ_{calcu} (N/m)	C_{11} (N/m)	C_{12} (N/m)	C_{66} (N/m)	Y (N/m)	ν
Tri-Tri arsenene	14.97	8.68	-6.55	13.92	21.30	6.53	7.38	19.30	0.31
Tri-Tri antimonen	12.24	10.04	-10.31	11.21	17.52	4.89	6.31	16.16	0.28

Table S2: Calculated effective masses (m), average effective masses (m_d), deformation potential (E_l), elastic modulus (C_{2D}), carrier mobilities (μ), relaxation times (τ) for monolayer Tri-Tri arsenene and Tri-Tri antimonene based on eq 1 at 300 K.

System	carrier type	m (G-X)	m/m_0 (G-K)	m_d	E_l	C_{2D}	μ	τ
		m_0	m_0	m_0	eV	eV/Å^2	cm^2/Vs	10^{-14}s
Tri-Tri arsenene	hole	0.82	0.73	0.77	0.39	0.73	2628.60	123.24
	electron	0.41	0.41	0.41	0.36	0.73	11524.78	268.86
Tri-Tri antimonene	hole	0.42	0.37	0.40	1.54	0.63	539.78	12.96
	electron	0.50	0.50	0.50	0.56	0.63	2789.63	78.89

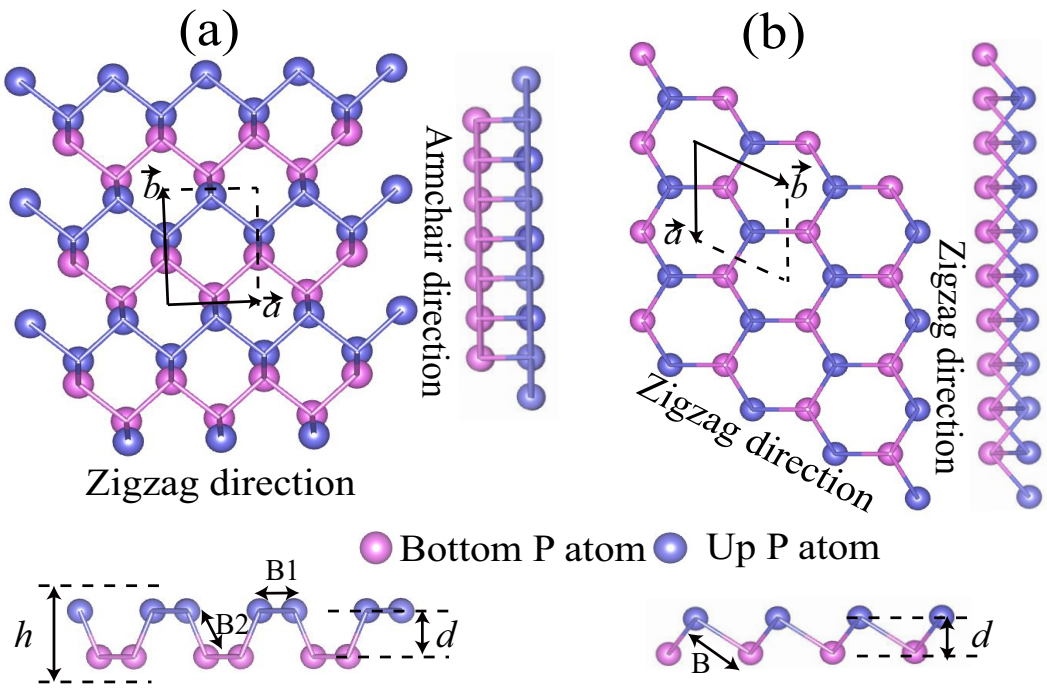

Fig.S1. Top and side views of the monolayer (a) black P and (b) blue P, where the top and bottom P sublattices in a nonplanar monolayer are represented by blue and red balls. Its unit cell is indicated by a black dashed line.

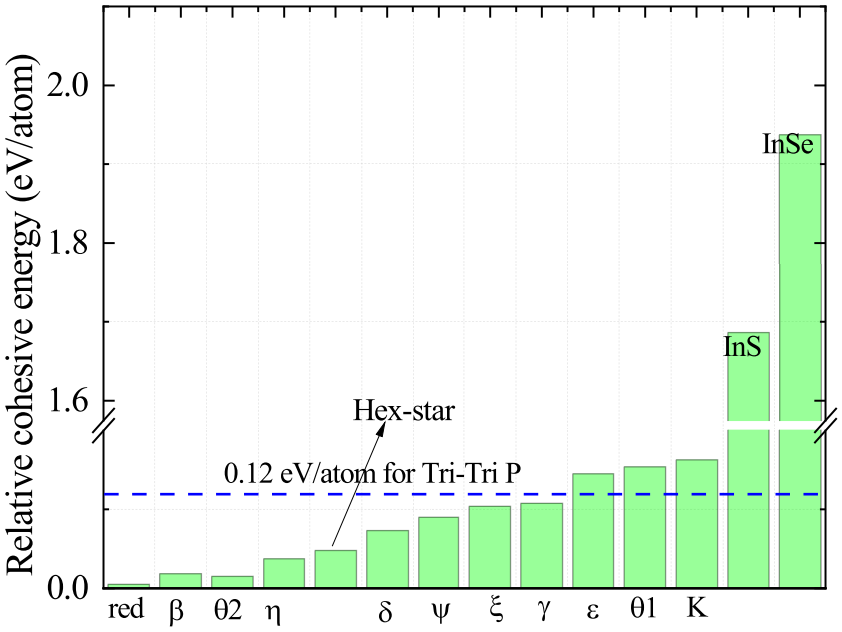

Fig.S2. The relative cohesive energies of some phosphorene allotropes and some other two-dimension materials, compared to black phosphorene.

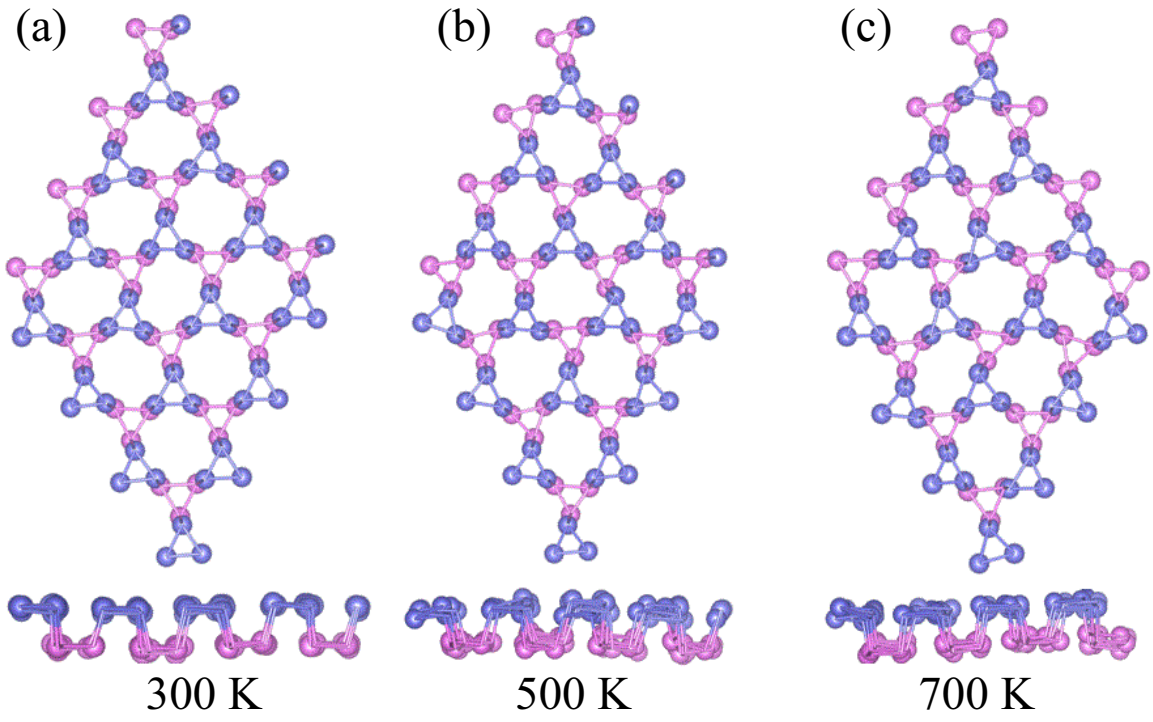

Fig.S3. The atomic configurations from the top view of the monolayer Tri-Tri P at the end of this AIMD simulation under 300 (a), 500 (b) and 700 K (c).

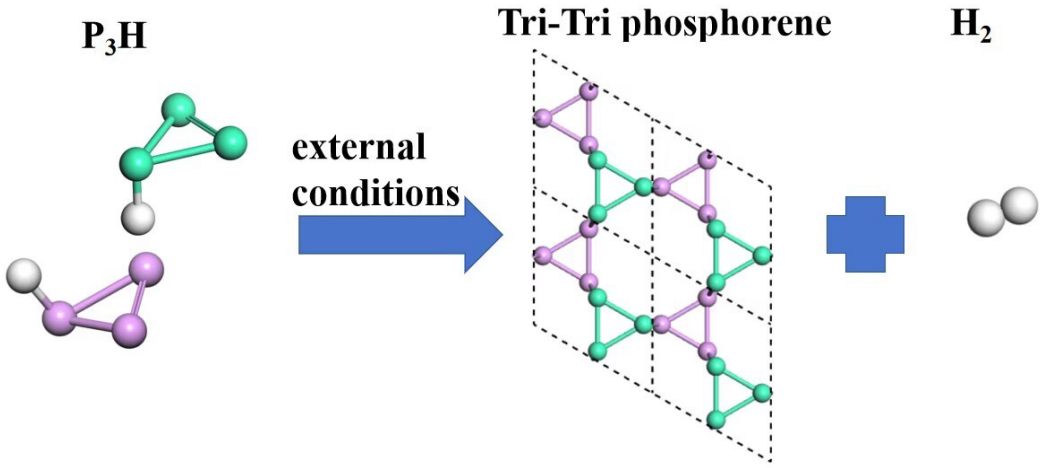

Fig.S4. The polyreaction of two 1H-Triphosphene (c-HP_3).

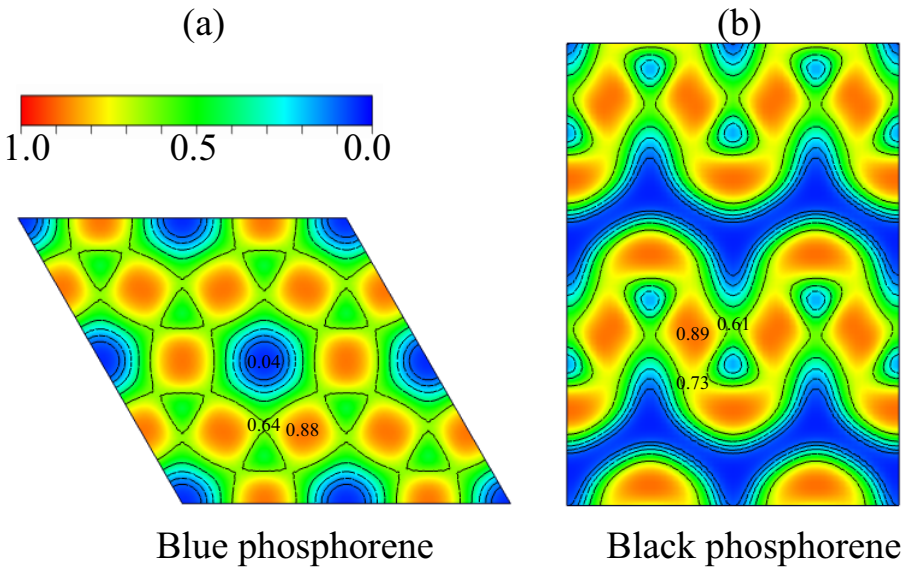

Fig.S5. The electron localized function (ELF) map of the monolayer black P (a) and blue P (b).

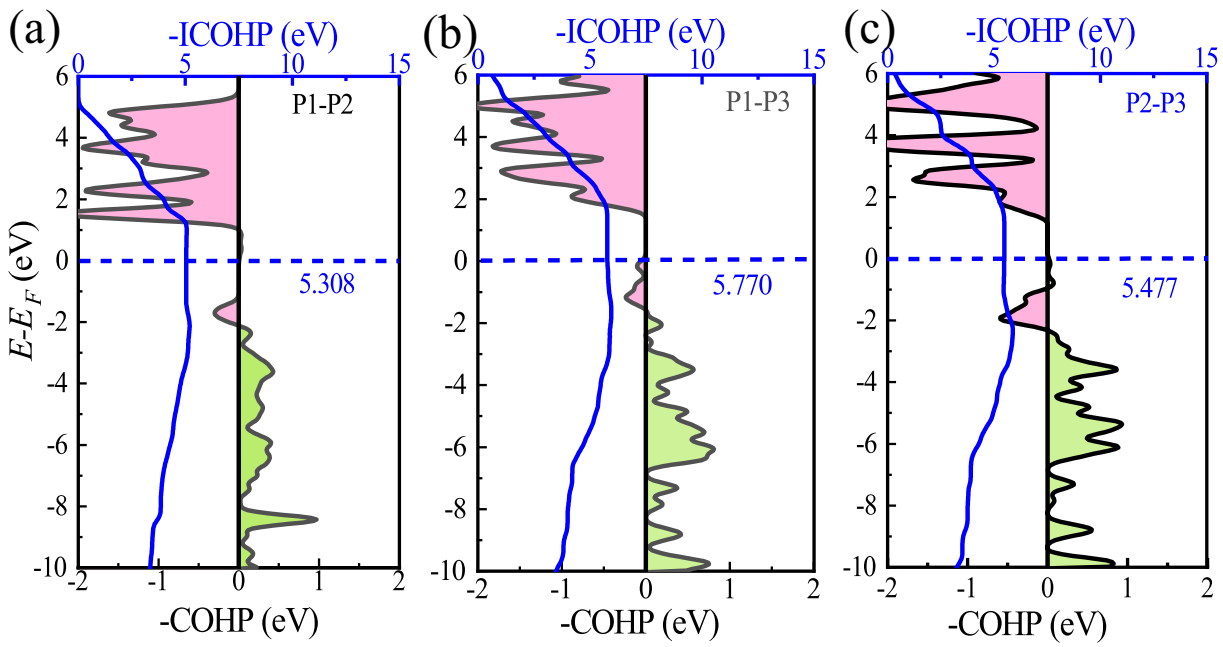

Fig.S6. The crystal orbital Hamilton population (COHP) analysis of P-P bonding in the monolayer blue P (a), and the monolayer black P (b) and (c). The blue line presents the integration of COHP, and the value of the COHP integration up to the Fermi level (ICOHP values in eV/bond) are listed as blue font.

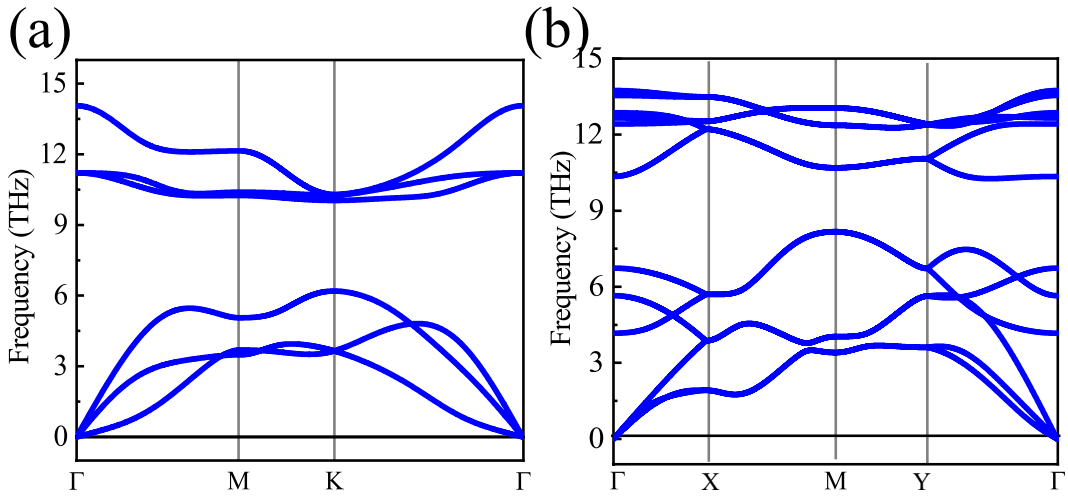

Fig.S7. Phonon spectra of the blue P (a) and black P (b).

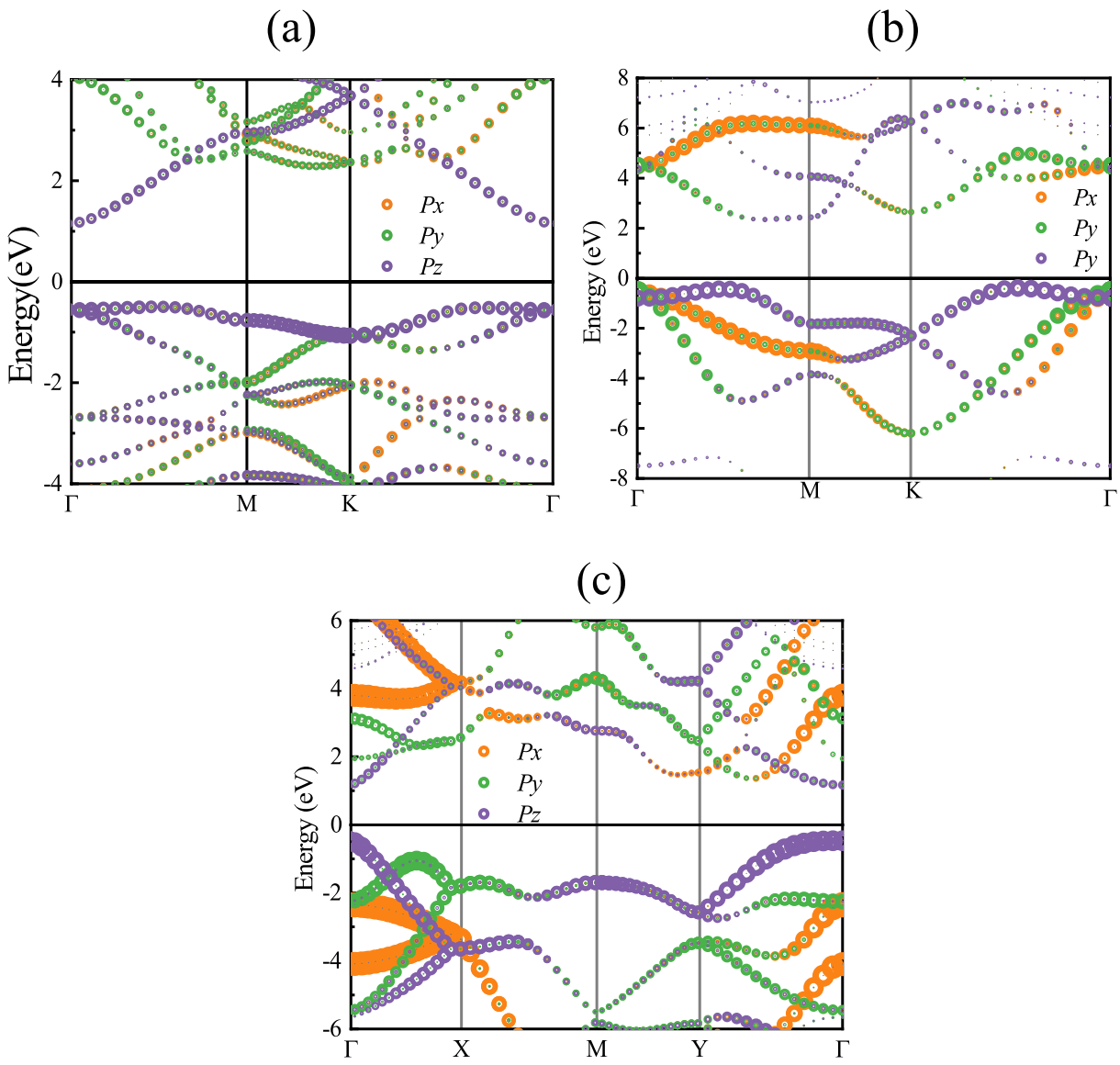

Fig.S8. The *px*, *py* and *pz* orbital-projected band structures of the monolayer Tri-Tri P (a), blue P (b), and black P (c).

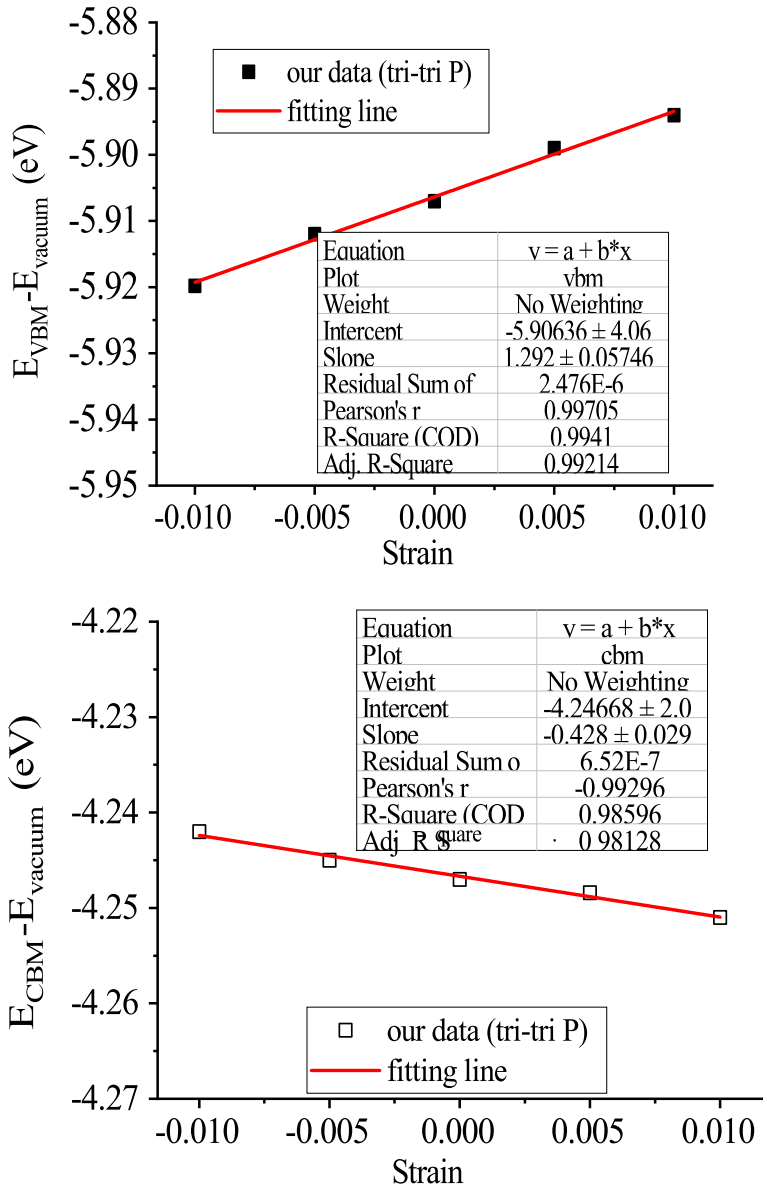

Fig.S9. Band energy of the CBM and VBM of monolayer Tri-Tri P with respect to the vacuum energy as a function of lattice deformation along *x* direction. Band energies were calculated with the HSE06 functional. Red solid lines are the fitting curves.

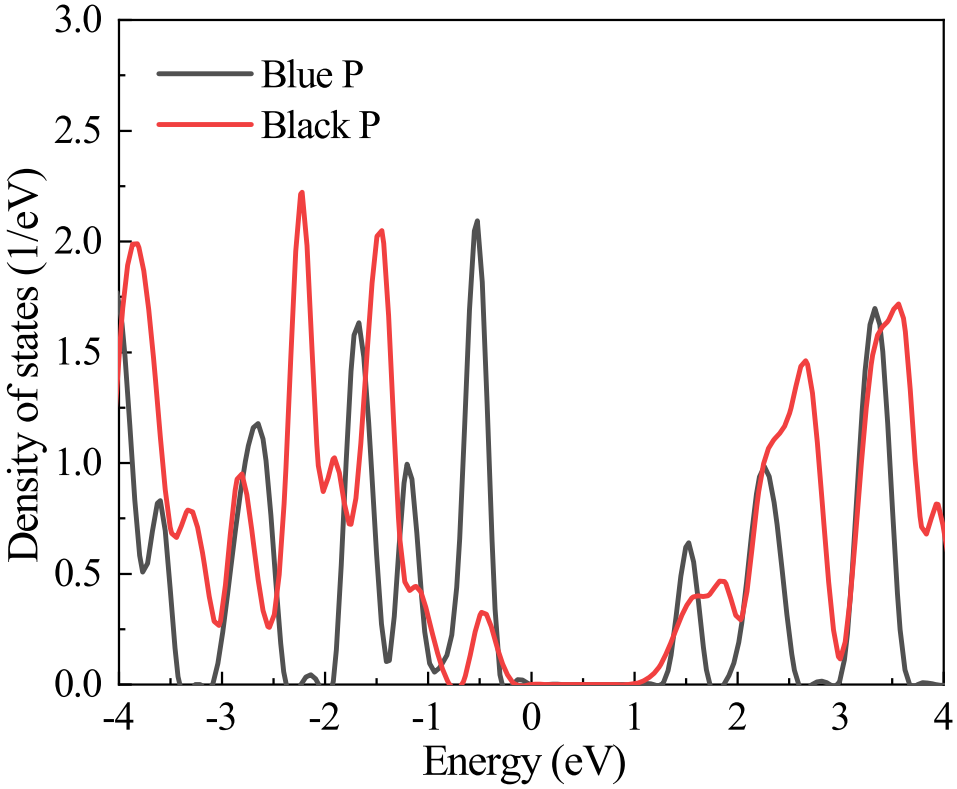

Fig.S10. The calculated total DOS of the monolayer black P and blue P.

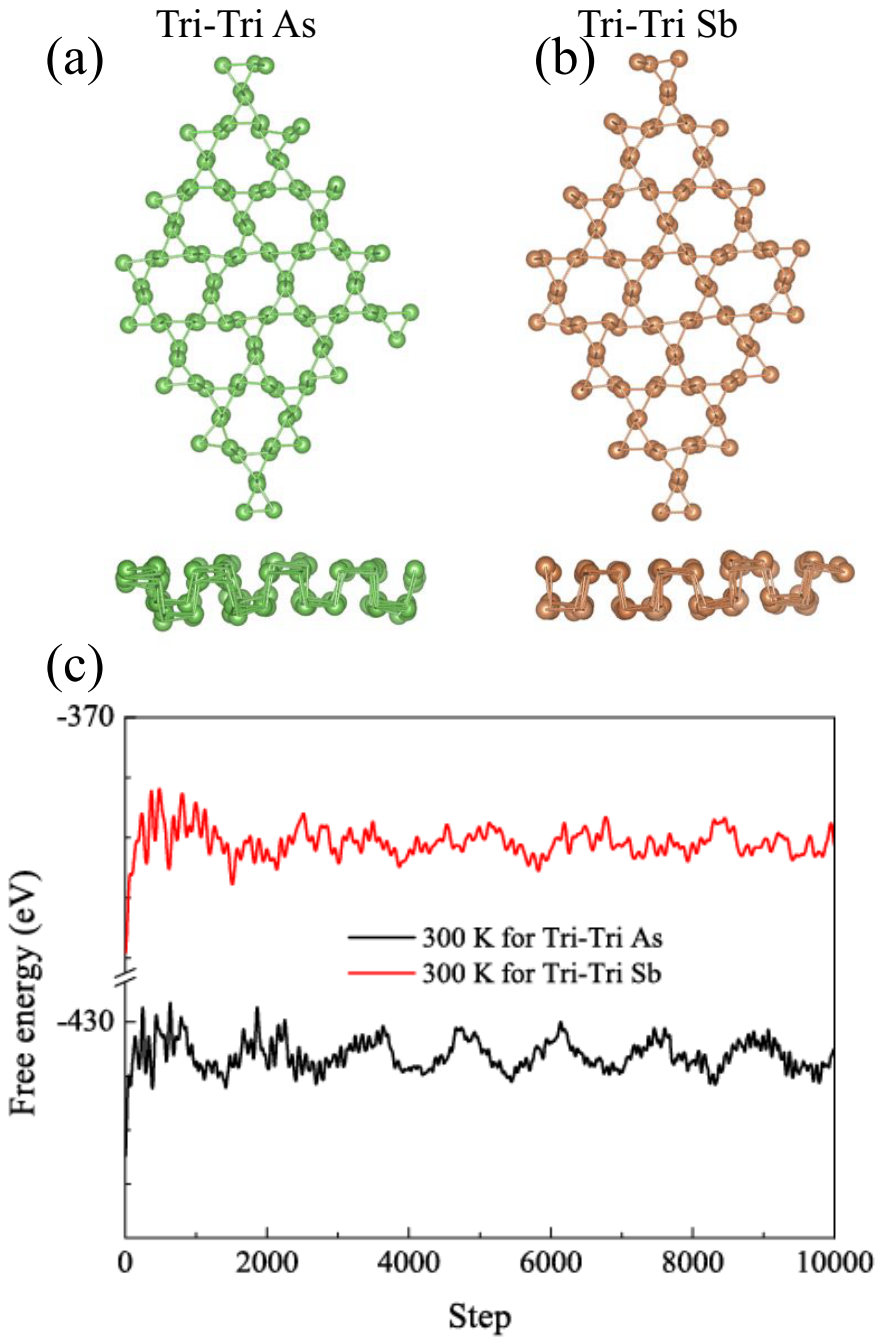

Fig.S11. The atomic configurations from the top view of the monolayer Tri-Tri As (a), and Tri-Tri Sb (b) at the end of this AIMD simulation under 300 K. (c) Evolution of total energy in the monolayer Tri-Tri As and Tri-Tri Sb during ab initio molecular dynamics simulation under 300 K.

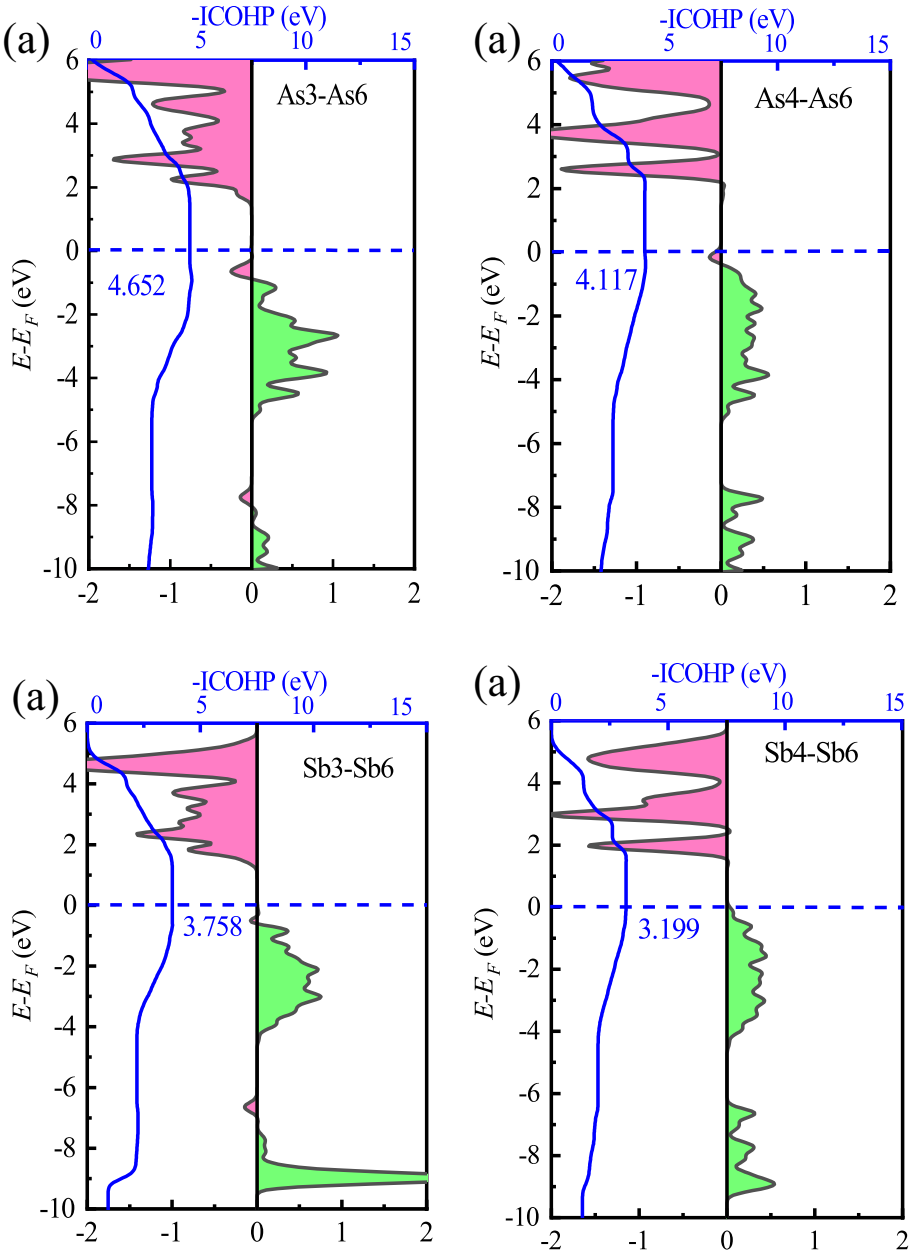

Fig.S12. The crystal orbital Hamilton population (COHP) analysis of B1 (a) and B2 bonding (b) in the monolayer Tri-Tri As. The COHP analysis of B1 (c) and B2 bonding (d) in the monolayer Tri-Tri Sb. The blue line presents the integration of COHP, and the value of the COHP integration up to the Fermi level (ICOHP values in eV/bond) are listed as blue font.

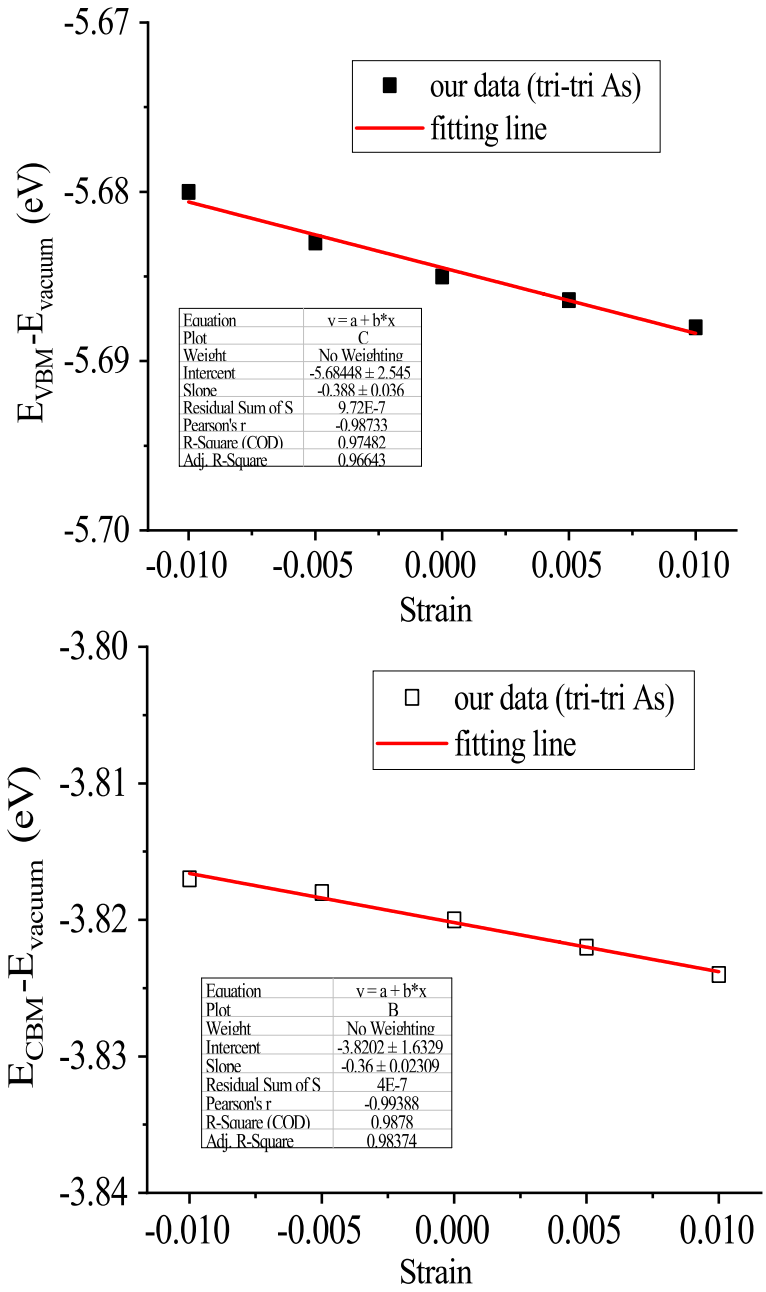

Fig.S13. Band energy of the CBM and VBM of monolayer Tri-Tri As with respect to the vacuum energy as a function of lattice deformation along *x* direction. Band energies were calculated with the HSE06 functional. Red solid lines are the fitting curves.

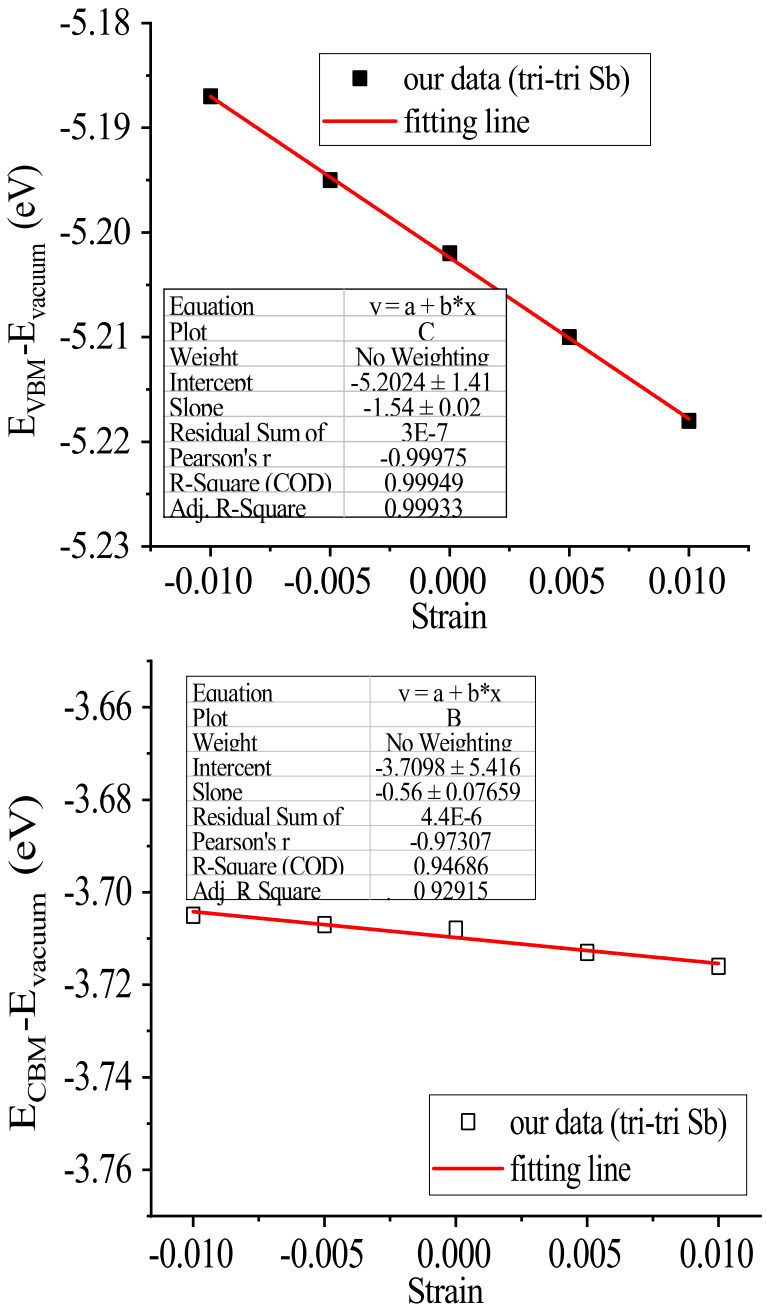

Fig.S14. Band energy of the CBM and VBM of monolayer Tri-Tri Sb with respect to the vacuum energy as a function of lattice deformation along *x* direction. Band energies were calculated with the HSE06 functional. Red solid lines are the fitting curves.